Mechanism of Transition-Metal Nanoparticle Catalytic Graphene Cutting

DATASET *in* JOURNAL OF PHYSICAL CHEMISTRY LETTERS · MARCH 2014

Impact Factor: 7.46 · DOI: 10.1021/jz500254u

THE JOURNAL OF PHYSICAL CHEMISTRY Letters

Letter

pubs.acs.org/JPCL

Mechanism of Transition-Metal Nanoparticle Catalytic Graphene Cutting

Liang Ma,[†] Jinlan Wang,*[,†] Joanne Yip,[‡] and Feng Ding[‡]

[†]Department of Physics & School of Chemistry and Chemical Engineering, Southeast University, Jiangning Campus, Nanjing 211189, China

[‡]Institute of Textiles and Clothing, Hong Kong Polytechnic University, Kowloon, Hong Kong, China

Supporting Information

ABSTRACT: Catalytic cutting by transition-metal (TM) particles is a promising method for the synthesizing of high-quality graphene quantum dots and nanoribbons with smooth edges. Experimentally, it is observed that the cutting always results in channels with zigzag (ZZ) or armchair (AC) edges. However, the driving force that is responsible for such a cutting behavior remains a puzzle. Here, by calculating the interfacial formation energies of the TM-graphene edges with ab initio method, we show that the surface of a catalyst particle tends to be aligned along either AC or ZZ direction of the graphene lattice, and thus the cutting of graphene is guided as such. The different cutting behaviors of various catalysts are well-explained based on the competition between TM-passivated graphene edges and the etching-agent-terminated ones. Furthermore, the kinetics of graphene catalytic cutting along ZZ and AC directions, respectively, are explored at the atomic level.

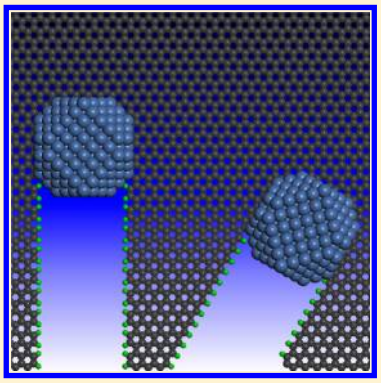

SECTION: Surfaces, Interfaces, Porous Materials, and Catalysis

Graphene is one of the most promising 2D materials for many advanced applications because it has exceptionally high-carrier mobility, structural stability, thermal conductivity, and mechanical strength.[1−4] Nanosized graphene, such as graphene nanoribbons (GNRs)[5−7] and graphene quantum dots (GQDs),[8,9] which edges its own intriguing electronic and magnetic properties, normally with tunable band gaps, can be used in spintronic and electronic devices, such as field-effect transistors[10,11] and in fast DNA sequencing.[12,13] To synthesize size- and edge-controllable GNRs and GQDs, numerous efforts have been dedicated to the development of graphene-cutting methods, such as sonochemical,[10,11] lithographic,[14−16] oxidation cutting techniques,[17−20] graphene nanocutting by using diamond-edge as knife,[21] and catalytic cutting by using the transition-metal (TM) nanoparticles.[22−34] Among these cutting methods, the catalytic cutting of graphene by TM nanoparticles holds the most promise for high-quality GNR or GQD fabrication due to the resultant well-defined and smooth edges.

In the environment with hydrogen gas and at an elevated temperature, a TM nanoparticle can catalyze the reaction of

$$G + 2H_2 \rightarrow G^* + CH_4 \quad (1)$$

where G and G* represent the uncut and cut graphene, respectively. In a controlled condition, the etching of the C atoms from graphene only occurs around the catalyst because the catalyst is able to (i) dissociate an H_2 molecule into two H radicals, (ii) weaken the nearby C−C bond in the graphene, and (iii) catalyze the formation of C−H bonds on the surface of TM nanoparticles.[32,35] Various metals, such as iron (Fe),[22,32] nickel (Ni),[23−26,32] cobalt (Co),[27,28,32] platinum (Pt),[29] and silver (Ag),[30] have been proven to be efficient to catalyze the graphene cutting (or unzipping), but the cutting behavior is catalyst-dependent. It was broadly observed that the channels cut by the use of Fe, Co, and Ni nanoparticles normally have either zigzag (ZZ) or armchair (AC) edges, and the changes in the cutting direction mostly lead to turns of 60 or 120°. This unique cutting behavior has great advantages for producing long and straight GNRs with well-defined edges, which is desirable for applications in graphene-based electronic and spintronic devices. However, the cutting of graphene by Ag nanoparticles in oxygen does not show a good control of the orientation, normally with a kinked orientation, and the width of the cut channel is much larger than the size of the catalyst particle. Although a phenomenological model has been proposed to understand the cutting process,[36] a deep insight into the control of the cutting direction and catalyst-dependent cutting behavior is not yet available.

By carefully modeling the TM particle−graphene interface and considering the role of hydrogen and oxygen in graphene-edge termination, our ab initio calculations demonstrate that such orientation selectivity arises from the energetically preferred interfaces between the TM nanoparticles and the ZZ or AC graphene edges. Moreover, the catalyst-dependent cutting behavior is explained as the result of the competition

Received: February 5, 2014
Accepted: March 18, 2014
Published: March 18, 2014

dx.doi.org/10.1021/jz500254u | J. Phys. Chem. Lett. 2014, 5, 1192−1197

between the metal−graphene interface and the hydrogen/oxygen termination of the graphene edges.

Experimental evidence has shown that the catalyst particles in graphene channels normally comprise a crystalline structure or are in the solid state,[27−29,37] and the angles between the facets are in multiples of 30°.[28,37] Thus it is reasonable to assume that the catalyst particles have polyhedral shapes with a few flat low-index facets that are in contact with the graphene. The surfaces of the catalyst particles may form various metal−graphene interfaces, such as the metal−ZZ and metal−AC interfaces, as shown in Figure 1 or the interfaces of metal−chiral graphene edges. Because of their large structural differences, these interfaces are expected to have different stabilities.

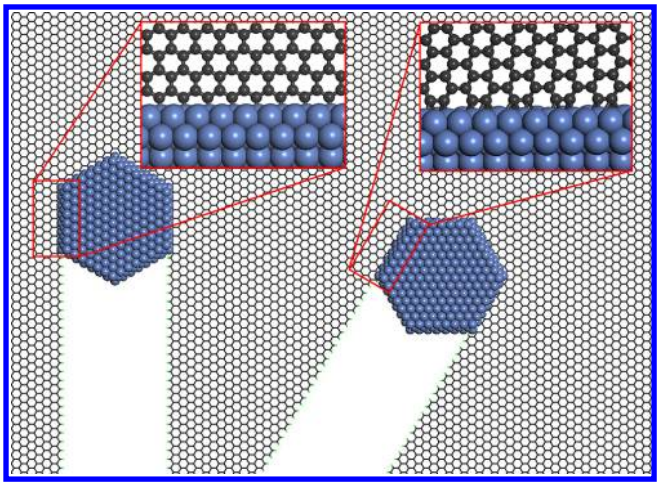

Figure 1. Catalytic cutting of graphene by metal nanoparticles along the zigzag (left) and armchair (right) edged channels and the corresponding metal−graphene interfaces. The inserts show the interfaces between the graphene and the catalyst particle.

To calculate the interfacial formation energy (FE) between graphene and the catalyst surface, we used GNRs with various edges attached to the surface of a three-layer TM(111) slab (as the (111) surface is the most stable one, see Table S1 in Supporting Information) to represent the catalyst−graphene interface (Figure 2). Another edge of the GNR is terminated by H atoms. A vector $\mathbf{R} = n\mathbf{a}_1 + m\mathbf{a}_2$ (where $\mathbf{a}_1$ and $\mathbf{a}_2$ are two basis vectors of the graphene lattice) or the chiral index (n, m), is used to denote the orientation of the graphene edge (Figure 2a). Similar to carbon nanotubes, $(n, 0)$ and (n, n) correspond to the ZZ and AC edges, respectively. The chiral angle θ of an edge is defined as the angle between vector $\mathbf{R}$ and the ZZ orientation of the graphene lattice, which fulfils:

$$\cos\theta = \frac{2n + m}{2\sqrt{n^2 + nm + m^2}} \quad (0° < \theta < 30°) \tag{2}$$

Seven different types of graphene edges, which are ZZ, (9,2), (4,1), (3,1), (2,1), (4,3), and AC, are considered, and four of them (ZZ, (9,2), (2,1), and AC) on the Ni(111) surface are shown in Figure 2b−e.

The FE of a TM(111)−graphene interface per unit of interfacial length (in nanometer) is defined as

$$FE_{\mathrm{TM-G}} = [E_{\mathrm{H\text{-}G\text{-}TM}} - E_{\mathrm{TM}} - N_{\mathrm{C}} \times E_{\mathrm{C}} - 1/2(E_{\mathrm{H\text{-}G\text{-}H}} - N_{\mathrm{C}} \times E_{\mathrm{C}})]/L \tag{3}$$

where $E_{\mathrm{H\text{-}G\text{-}TM}}$ and E_{TM} are the energies of the whole system and the TM(111) slab, respectively; N_{C} is the number of C atoms in the GNR and E_{C} is the energy of a C atom in the graphene; L is the length of the TM(111)−graphene interface in nanometers, $E_{\mathrm{H\text{-}G\text{-}H}}$ is the energy of the same GNR with both edges passivated by H atoms; and $1/2(E_{\mathrm{H\text{-}G\text{-}H}} - N_{\mathrm{C}} \times E_{\mathrm{C}})$ is the energy of an H-passivated graphene edge.

Stability of Graphene-Catalyst Interface and the Determination of the Cutting Direction. As shown in Figure 2f, the formation energies of the graphene edges attached to the (111) surface of Co, Ni, Cu, and Ag clearly show similar nonmonotonic dependence on the chiral angle of the graphene edge. The TM−ZZ and TM−AC interface are more stable than the ones near them and thus represent two local minima for all four

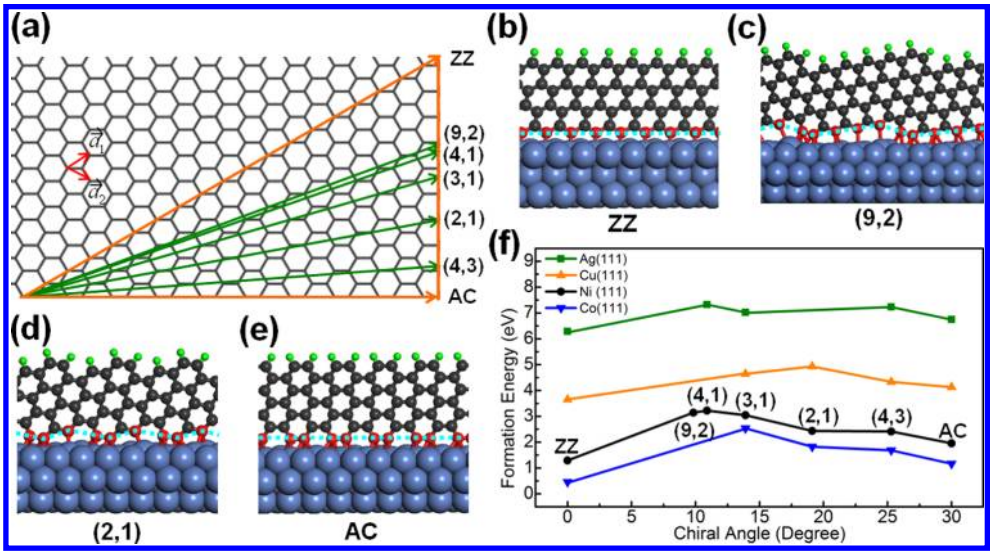

Figure 2. (a) Various graphene edges denoted by the chiral indexes (n, m) with respect to the basis vectors of the graphene lattice. (b−e) Graphene−Ni(111) interfaces where the edges of the graphene are ZZ, (9,2), (2,1), and AC, respectively. Green, black, and ultramarine balls represent H, C, and Ni atoms, respectively. The interfacial carbon atoms are highlighted in red. (f) Graphene−Ni(111), Co(111), Cu(111), and Ag(111) interfacial formation energies per unit of interfacial length (in nanometer) as a function of the chiral angle of the graphene edge.

dx.doi.org/10.1021/jz500254u | J. Phys. Chem. Lett. 2014, 5, 1192−1197

cases. The exceptional stability of the TM−ZZ and TM−AC interfaces can be attributed to the specific contact between the TM(111) surface and the graphene ZZ or AC edge. Because all of the atoms of the ZZ or AC edges are located in a straight line (Figure 2b,e), a strong binding between all of the edge atoms and the flat and densely packed TM (111) surface can be simultaneously achieved. In contrast, a chiral edge, such as (9,2) or (2,1), shows a kinky structure (Figure 2c,d), which can be viewed as a ZZ or AC edge with periodically distributed kinks. As a consequence of the appearance of the kinks, some edge atoms are closer to the TM(111) surface than others, and thus it is impossible to achieve strong binding between all graphene-edge atoms and a smooth catalyst surface. Such an arrangement of the edge atoms leads to fluctuations in both the edge C−TM distances and the C−TM binding strength. Among all potential graphene edges, only the ZZ and AC edges have atom arrangements along a linear edge and thus they represent the only two local minima in the FE versus θ curve.

It is important to note that such a discussion can be applied to other flat (e.g., (100)) metal surfaces and graphene edges. To validate this point, we further calculated the formation energies of Ni(100)−graphene interfaces. (See Figure S1 in the Supporting Information.) The result shown is similar to that of the Ni(111)−graphene interface: the Ni(100)−ZZ and Ni(100)−AC interfaces are two local minima of the FE versus θ curve.

Our calculation and analysis clearly establish that the flat surface of catalyst particles tends to be aligned along either the ZZ or AC direction in a graphene channel. Nevertheless, whether such an alignment is able to guide the graphene cutting along the ZZ or AC direction is still ambiguous. Figure 3 shows the formation of a hexagonal metal particle located in four cutting channels of graphene, where the cutting directions are ZZ, (9,2), (2,1), and AC, respectively. As previously mentioned, the surface of catalyst particles tends to form the energetically preferred TM−ZZ (in the channels along the ZZ and (9,2) directions) or TM−AC (in the channels along the AC and (2,1) directions) interfaces with the graphene, and thus the catalyst has only two favorable orientations, ZZ or AC, in a channel. As clearly seen in Figure 3a, four well-contacted metal−graphene interfaces are formed when the catalyst particles are in the ZZ or AC channel, but there are only three metal−graphene interfaces in the case of a chiral channel, such as (9,2) or (2,1). Clearly, if the metal−graphene interface is more stable than the etching-agent- (hydrogen or oxygen) terminated graphene edge (depending on the experimental conditions and will be clarified later), the catalyst particles would tend to be in the ZZ or AC channel. From the illustration of the formation energy of the catalyst particle as a function of the channel direction (Figure 3b), we can clearly see that the ZZ and AC channels correspond to two local minima. So, during the cutting of the graphene, even if the initial cutting channel is along a chiral direction, the catalyst would automatically adjust the orientation of the channel to either the ZZ or AC direction to achieve a more stable metal−graphene interface. It is important to note that the previous discussions and conclusions are still valid as long as the catalyst particle has two parallel flat crystal facets. (See Figures S2−S4 in the Supporting Information for illustrations of catalyst particles with other shapes (e.g., quadrilateral, octagon and dodecagon).)

Catalyst and Etching Agent-Dependent Cutting Behavior. The catalytic cutting of graphene by TMs such as Fe, Ni, and Co

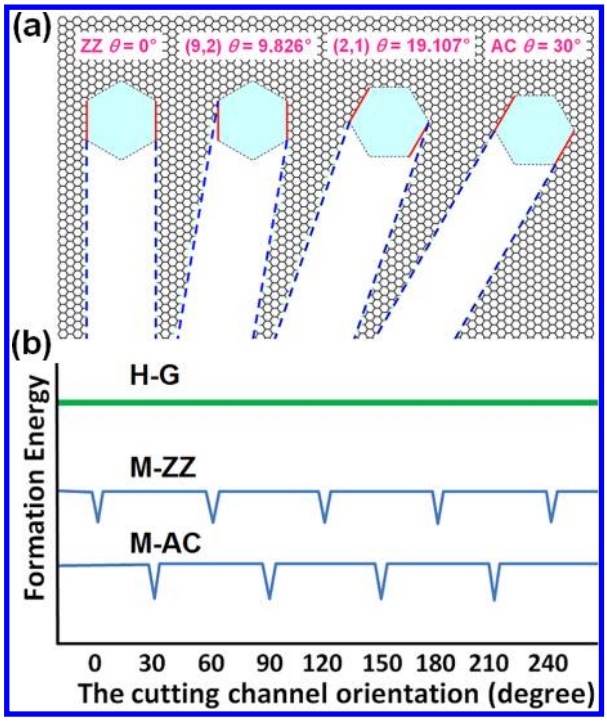

Figure 3. (a) Illustration of hexagonal catalyst nanoparticles in various graphene channels for θ = 0, 9.826, 19.107, and 30°, respectively. (b) Illustration of the formation energies of the catalyst particle-graphene interface as a function of the cutting channel orientation for H-terminated graphene edges (H-G), catalyst surface-terminated ZZ edges (M-ZZ), and catalyst surface-terminated AC edges (M-AC), respectively.

were mostly carried out in H_2 gas, and besides the etching of the C atoms, H also terminates the edges of the graphene channel. Thereby the competition between the metal−graphene interfaces and hydrogen-terminated graphene edges should also play an important role in the catalytic cutting of graphene. If the metal−graphene interface is more stable than the hydrogen-terminated graphene edge, the previous discussion is valid. If the hydrogen-terminated graphene edge is thermodynamically superior to the metal−graphene interface, H atoms should passivate all of the edges of the channels, and the scenario shown in Figure 3 is no longer valid.

Because the stability of metal−graphene interfaces depends on the type of catalyst, the cutting behavior must be catalyst-dependent as well. For example, it is known that Ni−C interaction is quite strong, while Ag−C interaction is rather weak.[38] Thus, the formation energy of the Ni−graphene interfaces is expected to be much smaller than that of the Ag−graphene interfaces, which is confirmed by our ab initio calculations (Figure 2f).

By carefully considering the free energy of H_2 gas and assuming that the hydrogen on the graphene edge is in thermal equilibrium with the H_2 gas, the competition between the Ni/Co/Cu/Ag-ZZ(AC) graphene interfacial formations and the hydrogen-terminated ZZ(AC) graphene edges is shown in Figure 4a. (The details of calculating the phase diagram are presented in the Supporting Information.) It is clear that the Ni/Co−graphene interface is more stable than the hydrogen-terminated graphene edge in a broad range (Figure 4a); in contrast, the Ag−graphene interface is less stable and only able to exist at very high temperatures and extremely low H_2 pressures; for example, T = 1200 K and $p_{H2} \leq 10^{-6}$ bar. On

dx.doi.org/10.1021/jz500254u | J. Phys. Chem. Lett. 2014, 5, 1192−1197

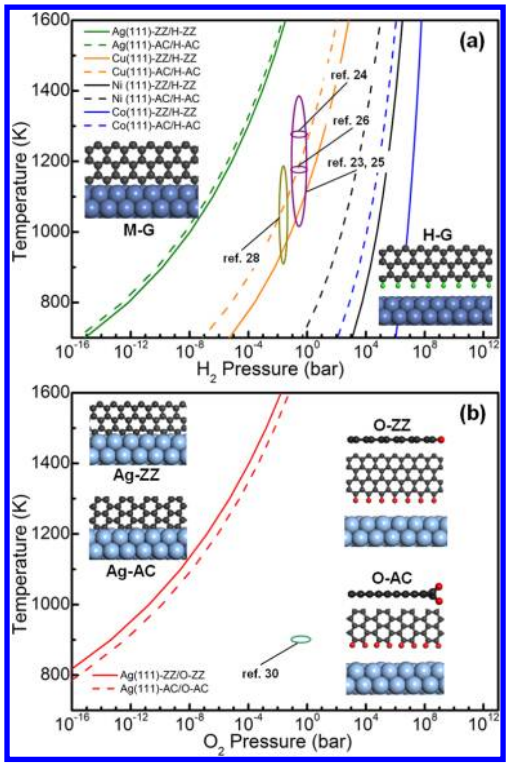

Figure 4. (a) Competition between metal-passivated graphene edges and the hydrogen-terminated edges. The insets show the metal−ZZ graphene (M-G) interface and H−ZZ graphene (H-G) edge, respectively. The purple and dark-yellow ellipses denote the experimental conditions of catalytic cutting of graphene by Ni[23−26] and Co,[28] respectively. (b) Competition between Ag(111)−ZZ(AC) interface and oxygen-passivated ZZ(AC) graphene edge. The insets show the Ag−ZZ(AC) interface and O−ZZ(AC) graphene edge. The green ellipse circle denotes the experimental conditions of Ag catalytic cutting of graphene in O_2 gas.[30]

the basis of this, the different cutting behavior between Ni/Co and Ag can be well understood. At a normal condition of cutting where the temperature is ∼900−1300 K and the pressure of H_2 is ∼1.0 bar, the Ni/Co−graphene interface is thermodynamically more stable than the H-terminated graphene edge, and thus the cutting along the ZZ or AC direction is expected. In contrast, the hydrogen-terminated graphene edge is more stable than the Ag−graphene; therefore, the graphene edges around the catalyst are preferred to be terminated by H atoms. In such a case, the binding between the catalyst and the graphene would be very weak, and the catalyst is able to diffuse inside the channel. So, the cutting channel must be much larger than the size of the catalyst particle, and no straight edge is expected. The activity of Cu is between Ni/Co and Ag, and thus both straight and waved cutting channels can be achievable by carefully tuning the hydrogen pressure if Cu is used as the catalyst.

In brief, the previous thermodynamic analysis shows that the capacities of these metals for cutting straight channels follow the order of Ag < Cu < Ni < Co, which is exactly the same as the order of their activity. Experimentally, the directional cutting behavior of Ni and Co was observed, as shown in refs 23−26 and 28.

Besides the dependence on the catalyst type, the cutting behavior also depends on the etching agent. Figure 4b shows the diagram of the oxygen terminated graphene AC/ZZ edges and the metal-passivated ones. Note that the oxygen and adjacent carbon atoms stagger alternately up and down at the oxygen-passivated AC graphene edge while the O−ZZ graphene edge shows a flat in-plane arrangement. It is transparent from the Figure that the Ag−graphene interface can only survive under extreme experimental condition (i.e., very low gas pressure when temperature below 1600 K) if O_2 is used as the etching agent. This suggests that the Ag cut graphene in O_2 normally should leave waved channels, as has been clearly seen in recent experiments.[30]

Atomic Processes of Catalytic Cutting. Although the cutting direction and the straight channel can be well understood by the above thermodynamic analysis, the details of the cutting at atomic level are still not clear. For example, etching carbon atoms away from AC and ZZ edges may be different from each other, and the difference can be identified by kinetic analysis only. To gain an insightful understanding on the graphene cutting kinetics, the etching of graphene edges in a repeatable manner is further explored. A ZZ GNR with four unit cell length (or eight carbon atoms on the edge forming a short zigzag chain) or a AC GNR with three unit cell length (or six edge carbon atoms forming three C−C pairs) on the Ni(111) surface is used in this study. The etching of a carbon atom occurs through two steps: (1) the dissociation of the C atom from graphene edge and its migration on the catalyst surface and (2) the removal of the dissociated C atom from the catalyst surface through the $C + 2H_2 \rightarrow CH_4$ reaction.

As clearly seen from Figures S5 and S6 in the Supporting Information, dissociating a C atom from the GNR edge normally leads to a significant increase in energy, while the hydrogenation of the dissociated C atom results in a large energy deduction. For the etching of ZZ graphene edge, the energy increasing of the first C atom dissociation is as high as 2.67 eV, which means high temperature is required to initiate such a cutting process. Once the first C atom is dissociated, the dissociation of others becomes easier until the four bottommost C atoms are removed. The dissociation of the second and third C atoms leads to an energy rising of 1.72 and 1.06 eV, respectively, and the dissociation of the fourth one causes an energy deduction of 0.48 eV. After the removal of the four bottommost atoms, the dissociation of the fifth atom from a flat configuration becomes energetically less favorable and the energy increase is 1.90 eV, which is higher than those in the following etching processes (1.65, 1.30, −0.24 eV, respectively). This indicates that the dissociation of the first C atom from the graphene ZZ edge is the threshold step of the cutting. The transition-state calculation indicates that the energy barrier of the first C atom dissociation from the ZZ edge is as high as 3.04 eV, and the barrier of its migration to the free catalyst surface is 1.47 eV (Figure S5 in the Supporting Information).

For the etching of AC edge, the energy increases during the dissociating the six edge C atoms are 2.15, 1.84, 1.28, 1.40, −0.34, −0.52 eV, respectively. The energy barrier of the first C atom dissociation from the AC edge is 3.67 eV (Figure S6 in the Supporting Information).

Considering the abundance of hydrogen and thermally excited nickel atoms on metal surface during the cutting, which normally occurred at very high temperature (∼1000−1300 K), we further explored the reaction routes with the presence of H atom or Ni atom. It is shown that with the assistance of the H atom or the Ni atom, the two barriers of the first C-atom dissociation from the ZZ edge are significantly reduced from 3.04 and 1.47 eV to 2.21 and 1.03 eV (Figure S7 in the

dx.doi.org/10.1021/jz500254u | J. Phys. Chem. Lett. 2014, 5, 1192−1197

Supporting Information) and to 1.67 and 0.97 eV (Figure S9 in the Supporting Information), respectively. Similarly, the barrier of the first C dissociation from the AC edge is reduced from 3.67 to 3.17 eV (Figure S8 in the Supporting Information) and 2.14 eV (Figure S10 in the Supporting Information), respectively. Thus, the first C-atom dissociation from a ZZ (AC) graphene edge can be achieved in less than 1 sec at an elevated temperature of ∼900 K or above (estimated by the transition-state theory, $t \approx 10^{-13}*\exp(E_b/kT) \approx 1$, where E_b = 2.29/2.14 eV).

In summary, we have explored the underlying mechanism of catalytic cutting of graphene by metal nanoparticles with the assistance of ab initio calculations. This study successfully addresses the research question on why catalytic cutting of graphene by metal particles is mostly along the ZZ or AC direction. Besides that, we have further revealed catalyst-dependent cutting where only the metals that strongly interact with graphene (e.g., Fe, Co, Ni, etc.) tend to cut graphene along either the ZZ or AC direction. In contrast, the metals that interact weakly with graphene (e.g., Cu, Ag, Au, etc.) tend to cut graphene that form channels larger than the catalyst particle size at random directions. We have also shown that proper operating temperatures and H_2 gas pressures can fine-tune the cutting behavior. Moreover, our theoretical predication derived from metal−graphene modeling shows perfect agreement with most experimental observations. These insightful understandings into the cutting mechanism can be used for better experimental designs for controllable GNR and GQD synthesis.

COMPUTATIONAL DETAILS

The spin-polarized density functional theory (DFT) calculations with the projected augmented wave (PAW) potentials[39] and the exchange-correlation functional based on the Perdew−Burke−Ernzerhof (PBE) generalized gradient approximation (GGA),[40] implemented in the Vienna ab initio simulation package (VASP),[41] were performed to calculate the interfacial formation energies. The substrate-supported GNR arrays were separated by ∼7 Å from each other, and a vacuum space of >10 Å was set to separate images along the z direction. The Brillouin zone integrations were sampled on a 3 × 3 × 1 k-point mesh for large supercells, and a denser 9 × 5 × 1 mesh was used for small cells. All structures were fully relaxed until the force components acting on each atom were smaller than 0.02 eV/Å. The energy cutoff for plane-wave basis sets was set to be 400 eV. We used the climbing-image nudged elastic band (CI-NEB) method to locate the minimum energy paths and the transition states.[42]

In the calculations, the supercells of TM(111) surfaces and achiral/chiral graphene edges were carefully selected to ensure that the lattice mismatches are <3% apart from the Cu(111)−ZZ interface. The lattice mismatch (∼3.85%) between Cu(111) surface and ZZ graphene edge requires an extremely large supercell to reduce lattice mismatch below 3%, making the calculation unfeasible. Instead, we compressed the Cu(111) by 3.12% and stretched the ZZ graphene edge by 0.78% to make them commensurate.

ASSOCIATED CONTENT

Supporting Information

Details of thermodynamic phase diagram, comparison of formation energies of metal surface with different index, the formation energies of Ni(100)−graphene interfaces, illustrations of the catalyst particles with quadrilateral, octagon, and dodecagon shapes in different graphene cutting channels, and the atomic kinetic processes of graphene catalytic cutting along ZZ and AC directions, respectively. This material is available free of charge via the Internet at http://pubs.acs.org.

AUTHOR INFORMATION

Corresponding Author

*E-mail: jlwang@seu.edu.cn.

Notes

The authors declare no competing financial interests.

ACKNOWLEDGMENTS

This work, carried out by the SEU, is supported by the NBRP (2010CB923401, 2011CB302004), NSFC (21173040, 21373045), the NSF of Jiangsu (BK20130016), SRFDP (20130092110029) of China, Scholarship Award for Excellent Doctoral Student of MOE of China, Research and Innovation Project for College Graduates of Jiangsu Province (CXZZ12_0087), and SEU (YBJJ1218). The work carried out by the Hong Kong Polytechnic University is supported by Hong Kong GRF(G-YX4Q), NSFC (21273189), and PolyU internal grant (B-Q26K, A-PM35, A-PK89, A-PJ50, G-YX4Q). The computational resources were provided by SEU and National Supercomputing Center in Tianjin.

REFERENCES

(1) Berger, C.; Song, Z.; Li, X.; Wu, X.; Brown, N.; Naud, C.; Mayou, D.; Li, T.; Hass, J.; Marchenkov, A. N.; et al. Electronic Confinement and Coherence in Patterned Epitaxial Graphene. *Science* **2006**, *312*, 1191−1196.

(2) Castro Neto, A. H.; Guinea, F.; Peres, N. M. R.; Novoselov, K. S.; Geim, A. K. The Electronic Properties of Graphene. *Rev. Mod. Phys.* **2009**, *81*, 109−162.

(3) Balandin, A. A.; Ghosh, S.; Bao, W. Z.; Calizo, I.; Teweldebrhan, D.; Miao, F.; Lau, C. N. Superior Thermal Conductivity of Single-Layer Graphene. *Nano Lett.* **2008**, *8*, 902−907.

(4) Lee, C.; Wei, X.; Kysar, J. W.; Hone, J. Measurement of the Elastic Properties and Intrinsic Strength of Monolayer Graphene. *Science* **2008**, *321*, 385−388.

(5) Son, Y.-W.; Cohen, M. L.; Louie, S. G. Energy Gaps in Graphene Nanoribbons. *Phys. Rev. Lett.* **2006**, *97*, 216803.

(6) Barone, V.; Hod, O.; Scuseria, G. E. Electronic Structure and Stability of Semiconducting Graphene Nanoribbons. *Nano Lett.* **2006**, *6*, 2748−2754.

(7) Zhu, L.; Wang, J.; Zhang, T.; Ma, L.; Lim, C. W.; Ding, F.; Zeng, X. C. Mechanically Robust Tri-Wing Graphene Nanoribbons with Tunable Electronic and Magnetic Properties. *Nano Lett.* **2010**, *10*, 494−498.

(8) Trauzettel, B.; Bulaev, D. V.; Loss, D.; Burkard, G. Spin Qubits in Graphene Quantum Dots. *Nat. Phys.* **2007**, *3*, 192−196.

(9) Ritter, K. A.; Lyding, J. W. The Influence of Edge Structure on the Electronic Properties of Graphene Quantum Dots and Nanoribbons. *Nat. Mater.* **2009**, *8*, 235−242.

(10) Li, X.; Wang, X.; Zhang, L.; Lee, S.; Dai, H. Chemically Derived, Ultrasmooth Graphene Nanoribbon Semiconductors. *Science* **2008**, *319*, 1229−1232.

(11) Wang, X.; Ouyang, Y.; Li, X.; Wang, H.; Guo, J.; Dai, H. Room-Temperature All-Semiconducting Sub-10-nm Graphene Nanoribbon Field-Effect Transistors. *Phys. Rev. Lett.* **2008**, *100*, 206803.

(12) Stine, R.; Robinson, J. T.; Sheehan, P. E.; Tamanaha, C. R. Real-Time DNA Detection Using Reduced Graphene Oxide Field Effect Transistors. *Adv. Mater.* **2010**, *22*, 5297−5300.

(13) Min, S. K.; Kim, W. Y.; Cho, Y.; Kim, K. S. Fast DNA Sequencing with a Graphene-Based Nanochannel Device. *Nat. Nanotechnol.* **2011**, *6*, 162−165.

(14) Han, M. Y.; Ozyilmaz, B.; Zhang, Y.; Kim, P. Energy Band-Gap Engineering of Graphene Nanoribbons. *Phys. Rev. Lett.* **2007**, *98*, 206805.
(15) Chen, Z.; Lin, Y.-M.; Rooks, M. J.; Avouris, P. Graphene Nano-ribbon Electronics. *Physica E* **2007**, *40*, 228−232.
(16) Jiao, L.; Zhang, L.; Wang, X.; Diankov, G.; Dai, H. Narrow Graphene Nanoribbons from Carbon Nanotubes. *Nature* **2009**, *458*, 877−880.
(17) McAllister, M. J.; Li, J.-L.; Adamson, D. H.; Schniepp, H. C.; Abdala, A. A.; Liu, J.; Herrera-Alonso, M.; Milius, D. L.; Car, R.; Prud'homme, R. K.; et al. Single Sheet Functionalized Graphene by Oxidation and Thermal Expansion of Graphite. *Chem. Mater.* **2007**, *19*, 4396−4404.
(18) Kosynkin, D. V.; Higginbotham, A. L.; Sinitskii, A.; Lomeda, J. R.; Dimiev, A.; Price, B. K.; Tour, J. M. Longitudinal Unzipping of Carbon Nanotubes to form Graphene Nanoribbons. *Nature* **2009**, *458*, 872−876.
(19) Fujii, S.; Enoki, T. Cutting of Oxidized Graphene into Nanosized Pieces. *J. Am. Chem. Soc.* **2010**, *132*, 10034−10041.
(20) Ma, L.; Wang, J.; Ding, F. Strain-Induced Orientation-Selective Cutting of Graphene into Graphene Nanoribbons on Oxidation. *Angew. Chem., Int. Ed.* **2012**, *51*, 1161−1164.
(21) Mohanty, N.; Moore, D.; Xu, Z.; Sreeprasad, T. S.; Nagaraja, A.; Rodriguez, A. A.; Berry, V. Nanotomy-Based Production of Transferable and Dispersible Graphene Nanostructures of Controlled Shape and Size. *Nat. Commun.* **2012**, *3*, 844.
(22) Datta, S. S.; Strachan, D. R.; Khamis, S. M.; Charlie Johnson, A. T. Crystallographic Etching of Few-Layer Graphene. *Nano Lett.* **2008**, *8*, 1912−1915.
(23) Ci, L.; Xu, Z.; Wang, L.; Gao, W.; Ding, F.; Kelly, K. F.; Yakobson, B. I.; Ajayan, P. M. Controlled Nanocutting of Graphene. *Nano Res.* **2008**, *1*, 116−122.
(24) Campos, L. C.; Manfrinato, V. R.; Sanchez-Yamagishi, J. D.; Kong, J.; Jarillo-Herrero, P. Anisotropic Etching and Nanoribbon Formation in Single-Layer Graphene. *Nano Lett.* **2009**, *9*, 2600−2604.
(25) Ci, L.; Song, L.; Jariwala, D.; Elias, A. L.; Gao, W.; Terrones, M.; Ajayan, P. M. Graphene Shape Control by Multistage Cutting and Transfer. *Adv. Mater.* **2009**, *21*, 4487−4491.
(26) Lukas, M.; Meded, V.; Vijayaraghavan, A.; Song, L.; Ajayan, P. M.; Fink, K.; Wenzel, W.; Krupke, R. Catalytic Subsurface Etching of Nanoscale Channels in Graphite. *Nat. Commun.* **2013**, *4*, 1379.
(27) Konishi, S.; Sugimoto, W.; Murakami, Y.; Takasu, Y. Catalytic Creation of Channels in the Surface Layers of Highly Oriented Pyrolytic Graphite by Cobalt Nanoparticles. *Carbon* **2006**, *44*, 2338−2340.
(28) Schaffel, F.; Warner, J. H.; Bachmatiuk, A.; Rellinghaus, B.; Buchner, B.; Schultz, L.; Rummeli, M. H. Shedding Light on the Crystallographic Etching of Multi-Layer Graphene at the Atomic Scale. *Nano Res.* **2009**, *2*, 695−705.
(29) Santiesteban, J.; Fuentes, S.; Yacaman, M. J. Catalysis of Carbon Methanation by Small Platinum Particles. *J. Vac. Sci. Technol., A* **1983**, *1*, 1198−1200.
(30) Severin, N.; Kirstein, S.; Sokolov, I. M.; Rabe, J. P. Rapid Trench Channeling of Graphenes with Catalytic Silver Nanoparticles. *Nano Lett.* **2009**, *9*, 457−461.
(31) Wang, J.; Ma, L.; Yuan, Q.; Zhu, L.; Ding, F. Transition-Metal-Catalyzed Unzipping of Single-Walled Carbon Nanotubes into Narrow Graphene Nanoribbons at Low Temperature. *Angew. Chem., Int. Ed.* **2011**, *50*, 8041−8045.
(32) Tomita, A.; Tamai, Y. Optical Microscopic Study on the Catalytic Hydrogenation of Graphite. *J. Phys. Chem.* **1974**, *78*, 2254−2258.
(33) Ma, L.; Wang, J.; Ding, F. Recent Progress and Challenges in Graphene Nanoribbon Synthesis. *ChemPhysChem* **2013**, *14*, 47−54.
(34) Zoberbier, T.; Chamberlain, T. W.; Biskupek, J.; Kuganathan, N.; Eyhusen, S.; Bichoutskaia, E.; Kaiser, U.; Khlobystov, A. N. Interactions and Reactions of Transition Metal Clusters with the Interior of Single-Walled Carbon Nanotubes Imaged at the Atomic Scale. *J. Am. Chem. Soc.* **2012**, *134*, 3073−3079.
(35) Goethel, P. J.; Yang, R. T. Mechanism of Graphite Hydrogenation Catalyzed by Nickel. *J. Catal.* **1987**, *108*, 356−363.
(36) Datta, S. S. Wetting and Energetics in Nanoparticle Etching of Graphene. *J. Appl. Phys.* **2010**, *108*, 024307.
(37) Wang, H.; Li, K.; Yao, Y.; Wang, Q.; Cheng, Y.; Schwingenschlogl, U.; Zhang, X. X.; Yang, W. Unraveling the Atomic Structure of Ultrafine Iron Clusters. *Sci. Rep.* **2012**, *2*, 995.
(38) Ding, J.; Qiao, Z.; Feng, W.; Yao, Y.; Niu, Q. Engineering Quantum Anomalous/Valley Hall States in Graphene via Metal-atom Adsorption: An Ab-initio Study. *Phys. Rev. B* **2011**, *84*, 195444.
(39) Blochl, P. E. Projector Augmented-Wave Method. *Phys. Rev. B* **1994**, *50*, 17953−17979.
(40) Perdew, J. P.; Burke, K.; Ernzerhof, M. Generalized Gradient Approximation Made Simple. *Phys. Rev. Lett.* **1996**, *77*, 3865−3868.
(41) Kresse, G.; Hafner, J. Ab Initio Molecular Dynamics for Open-Shell Transition Metals. *Phys. Rev. B* **1993**, *48*, 13115−13118.
(42) Henkelman, G.; Uberuaga, B. P.; Jonsson, H. A Climbing Image Nudged Elastic Band Method for Finding Saddle Points and Minimum Energy Paths. *J. Chem. Phys.* **2000**, *113*, 9901−9904.